BORON REMOVAL FROM HYDRAULIC FRACTURING WASTEWATER USING CONVENTIONAL ALUMINUM AND IRON COAGULATION: PROCESSES AND UPTAKE MECHANISMS

A Thesis

by

DARPAN ATUL CHORGHE

Submitted to the Office of Graduate and Professional Studies of
Texas A&M University
in partial fulfillment of the requirements for the degree of

MASTER OF SCIENCE

Chair of Committee,   Shankararaman Chellam
Committee Members,   Gretchen Miller
                      Youjun Deng

Head of Department,   Robin Autenrieth

May 2017

Major Subject: Civil Engineering

ABSTRACT

One promising strategy to manage the large volumes of water needed for and wastewater generated by hydraulic fracturing is on-site treatment and reuse. In particular, the saline flowback water contains many of the chemicals employed for fracking, which need to be removed before possible reuse as "frac water." This manuscript targets one chemical of concern: borate based cross-linkers. To this end, coagulation-flocculation-sedimentation was evaluated for boron removal from saline flowback water obtained from a well in the Eagle Ford shale. Very high dosages reaching Al/B and Fe/B ratios of ~70 were necessary to remove ~80% boron at an optimal pH of 8. X-ray photoelectron spectroscopy revealed B-O bonding on surfaces of freshly precipitated $Al(OH)_3$(am) and $Fe(OH)_3$(am) suggesting boron uptake was predominantly via ligand exchange. Attenuated total reflection-Fourier transform infra-red (ATR-FTIR) spectroscopy provided direct evidence of inner- and outer-sphere boron complexation with coagulant surface hydroxyl groups. Only trigonal boron was detected on aluminum flocs since possible presence of tetrahedral boron was masked by severe Al-O-Al and Al-O interferences. In contrast, both trigonal and tetrahedral conformation of boron complexes was identified on $Fe(OH)_3$ surfaces. Direct Al-B or Fe-B bonding was not observed demonstrating boron was complexed largely with surface hydroxyl groups. Considering vast complexity of flowback water, it is important to develop in-depth understanding of chemistry of different flowback components like organic carbon compounds, silica compounds to scale up this bench scale experiment on an industrial level.

ACKNOWLEDGEMENTS

Firstly, I would like to express my gratitude to my thesis advisor Dr. Shankar Chellam for providing me this opportunity of doing world-class research. I am thankful to him for his continuous support, motivation, guidance and immense knowledge. His teaching style and enthusiasm aroused in me the interest to undertake research. I couldn't have imagined a better advisor than him. He was instrumental in not just shaping my thesis but also my personality as a whole.

Besides Dr. Chellam, I would like to thank the rest of my thesis committee: Dr. Gretchen Miller and Dr. Youjun Deng for their insightful comments and questions which encouraged me to further widen my research from different perspectives.

My sincere thanks also goes to Mutiara Ayu Sari for her unconditional support and advice at every step during my research. Without her precious support it would not have been possible to conduct this research. I am also grateful to my fellow lab mates and friends for continuous motivation and stimulating discussions.

I take this opportunity to express my gratitude to everyone who has contributed directly or indirectly towards this research.

Last but not the least, this would not have been possible without the support from my parents, my grandparents and my brother. This thesis is a testimony to their love and encouragement.

CONTRIBUTORS AND FUNDING SOURCES

Contributors

This work was supervised by a thesis committee headed by Dr. Shankararaman Chellam along with members Dr. Gretchen Miller and Dr. Youjun Deng.

X-ray Diffraction analysis for this project was done in Dr. Youjun Deng's soil minerology lab with the help of his PhD student Chun-Chun. The XRD data was interpreted using Dr. Deng's and Chun-Chun's help. XPS analysis for this research project was conducted in the Material Characterization facility at Texas A & M University. The data obtained from XPS and ATR-FTIR spectroscopy was analyzed using Mutiara Ayu's help. The highly magnified TEM images of the coagulant flocs were obtained from the Microscopy Imaging Center at Texas A & M University.

All other work conducted for the thesis was completed by the student independently.

Funding Sources

NOMENCLATURE

ATR-FTIR	Attenuated Total Reflectance-Fourier Transform Infrared
XPS	X-ray Photoelectron Spectroscopy
DOC	Dissolved Organic Carbon
TDS	Total Dissolved Solids
TSS	Total Suspended Solids
ICP-OES	Inductively Coupled Plasma-Optical Emission Spectroscopy
TEM	Transmission Electron Microscopy
SEM	Scanning Electron Microscopy

TABLE OF CONTENTS

LIST OF FIGURES

LIST OF TABLES

1.   INTRODUCTION

Unconventional oil and gas exploration and production by hydraulic fracturing requires large volumes of water [1], each well requiring an estimated 10 – 20 million liters [2]. Concomitantly, copious amounts of wastewater contaminated by myriad chemicals in spent fracturing fluids [3] and those naturally present in the subsurface are generated, making water management a critical issue [4]. Additionally, increasing scrutiny by regulatory agencies and the public at large as well as the high costs, noise, and spills associated with transporting water and wastewater has prompted research into on-site purification of wastewater and reuse it for additional fracturing [4, 5]. In particular, the water flowing to the surface over the first few days to weeks after fracking is highly saline and contains relatively high concentrations of the additives employed for fracking [2, 4, 6]. Hence, this "flowback water" requires treatment to remove suspended solids, organic matter, inorganic cross-linkers, friction reducers, corrosion/scale inhibitors, and biocides before possible reuse [2, 4, 7, 8]. Specifically, this research targets chemical coagulation to remove boron originally added in the form of borate based cross-linkers (along with Guar gum) to impart favorable rheological characteristics to the frack fluid [3, 9].

Boron is an essential micronutrient for plants and potentially even for humans. However, at higher concentrations, it is toxic to many crops and fruits [10] and consequently needs to be controlled to low levels in irrigation water. Additionally, animals exhibit developmental and reproductive toxicity following chronic exposure to boron, which induces teratogenic effects as well as testicular lesions, shrunken scrota,

1

and lowered body weights [11, 12]. Although human exposure to boron in the United States is deemed too low for setting maximum contaminant levels in drinking water [13], the World Health Organization (WHO) has recommended a provisional guideline of 0.5 mg/L. Hence, boron is one of the chemicals of concern that needs to be removed from the flowback/produced water before it can be reused for irrigation or further fracking or discharged into the environment.

To date, several technologies such as ion exchange, reverse osmosis, nanofiltration, and adsorption and have been shown to be capable of removing boron from contaminated waste streams [14-18]. Since layered double hydroxides and aluminum electrocoagulants are effective in adsorbing boron [19, 20], we hypothesized that conventional chemical coagulation would also be a cost-effective and facile option. Hydrolyzing aluminum and ferric salts are commonly employed as coagulants to remove turbidity (suspended solids), organic matter, microorganisms, arsenic, and other contaminants during conventional municipal water and wastewater treatment [21]. They have also been shown to be effective in removing naphthenic acids, barium, and vanadium from wastewater generated from oil sands operations [22]. Recently, there has been much interest in evaluating a closely related process, electrocoagulation for boron removal. The vast majority of such investigations have focused on optimizing electrocoagulation process parameters such as pH, coagulant type and dosage, current density, charge loading, contact time, and electrode spacing to maximize boron removal from a variety of feed streams including produced water [23], synthetic solutions [24, 25], and geothermal waters [26]. However, its effectiveness for clarifying hydraulic

fracturing wastewater is only beginning to be investigated. Importantly, boron removal specifically has not yet been established [7]. Boron adsorption onto iron and aluminum hydroxides has been reported to be endothermic [27, 28] and shown to decrease with increasing concentrations of anions such as carbonate, phosphate, and arsenate [28]. We recently demonstrated a ligand exchange mechanism for boron uptake onto electrochemically generated $Al(OH)_3$ and the presence of planar trigonal boron on aluminum flocs [20]. To our knowledge, no systematic investigations of conventional chemical coagulation to remove boron from saline flowback/produced waters are available.

The objectives of this research are to (i) evaluate alum and ferric chloride as coagulants to remove boron, turbidity and other flowback/produced water components, (ii) show direct evidence of boron adsorption onto freshly precipitated $Al(OH)_3$ and $Fe(OH)_3$ and elucidate associated uptake mechanisms, and (iii) provide clues to the conformation and geometry of boron adsorbed on flocs. Jar tests were performed with a flowback water sample from the Eagle Ford shale play in Texas over a range of pH (6 – 9) values and dosages (0 – 9 g/L). Floc surfaces were examined by X-ray photoelectron spectroscopy (XPS) and attenuated total reflection-Fourier transform infra-red (ATR-FTIR) spectroscopy to characterize boron surface complexes.

2.   MATERIALS AND METHODS

2.1. Source water characteristics including boron concentration. A flowback water sample from one of the most heavily drilled sites in the United States, the Eagle Ford formation in South Texas was used [29, 30]. Its physiochemical characteristics measured using inductively coupled plasma – optical emission spectroscopy (ICP-OES), titration, and other methods are summarized in Table 1. Turbidity was measured using a Hach ratio turbidimeter (model 2100N), the total suspended solids and total dissolved solids concentrations were measured gravimetrically by drying 25 mL of sample to dryness. The dissolved organic carbon was measured by the combustion-infrared method using a Shimadzu TOC-L instrument. Chloride, silica, ammonia, sulfate, calcium hardness, total hardness, and alkalinity were all quantified by colorimetric titrations (Hach method 8207, 8012, 8038, 8051, 8204, 8213, and 8203 respectively). Average values and standard deviations of three replicate measurements are shown in Table 1.

Table 1. Summary of important physicochemical parameters of the flowback water

Parameter	Unit	Concentration or value
pH	-	7.8 ± 0.2
Turbidity	NTU	117 ± 15
UV_{254}	cm^{-1}	2.41 ± 0.1
Total suspended solids (TSS)	mg/L	220 ± 1.4
Total dissolved solids (TDS)	mg/L	$28,700 \pm 180$
Dissolved organic carbon (DOC)	mg/L	$1,090 \pm 112$
Total Hardness	mg/L as $CaCO_3$	$2,890 \pm 180$
Ca Hardness	mg/L as $CaCO_3$	$2,520 \pm 32$
Alkalinity	mg/L as $CaCO_3$	345 ± 11.5
SiO_2	mg/L	181 ± 16
Cl^-	mg/L	$20,406 \pm 1040$
Fe	mg/L	0.3 ± 0.015
B	mg/L	132 ± 1.9
Na	mg/L	$8,997 \pm 670$
Al	mg/L	< 0.5
Ba	mg/L	8.5 ± 1.3
Ca	mg/L	$1,095 \pm 21$
Mg	mg/L	459 ± 8
P	mg/L as PO_4^{-3}	1.1 ± 0.20
Ammonia	mg/L	0.4 ± 0.01
Sulfate	mg/L	67 ± 1.5

As shown in Table 1, the flowback water was very saline (high TDS), turbid, well-buffered, hard, and high in organic carbon, calcium, and silica content, consistent with the frac-water formulation and its geological origins in predominantly limestone, marlstone, grainstone, bentonite, and shale [29, 30]. The measured boron concentration (132 mg/L) was higher than other produced waters [15, 27, 31] but similar to our recent report from Eagle Ford [20]. Ammonia, phosphate, aluminum, and iron concentrations were low, facilitating potentiometric titrations to measure boron [32]. In this technique, aqueous boron concentrations were determined by first adding $KMnO_4$ and EDTA to break any organo-boron bonds, oxidize to borate, and chelate interferences. This was

important since trivalent ions (aluminum and iron) were added as coagulants. D-mannitol was then added to produce an acid complex, which was then titrated using 0.02 N NaOH. The water sample was also characterized using ATR-FTIR and XPS as reported in section 3.1.

Additionally, a model solution with TDS and boron concentrations similar to the flowback water (28,000 mg/L NaCl and 120 mg/L boron) was formulated to perform preliminary experiments to optimize coagulation conditions and as a negative control to verify boron spectral peak assignment by eliminating potential interferences from other produced water components during instrumental measurements.

2.2. Coagulation. Experiments were performed using a programmable jar tester (Model-PB 90, Phipps and Bird Inc., Richmond, VA) with 1-L water adjusted to pH values of 6, 8, and 9 ($\pm$ 0.2) in a wide range of dosages (0 – 9,000 mg/L) using aluminum sulfate and iron chloride. A photograph of the jar testing apparatus is shown in Appendix A. The pH was maintained at the targeted values using NaOH. Samples were rapidly mixed at 150 s^{-1} for 2 minutes, flocculated at 45 s^{-1} for 30 minutes, and allowed to settle for 30 minutes. 100 mL of supernatant was taken to measure boron, turbidity, and DOC removal. Photographs of the untreated flowback water sample and jars after coagulation, flocculation, and sedimentation are given in Appendix B. Flocs were harvested by centrifugation at 2,000 rpm for 20 minutes, vacuum dried, and ground using an agate mortar and pestle before spectroscopy.

2.3. ATR-FTIR. Spectra in the range 4000 – 650 cm^{-1} were collected using a Nicolet iS10 spectrometer equipped with mid infrared Ever-Glo source, DTGS detector, KBr

beam splitter and Omnic 9.0 software. A diamond iTX accessory was installed to allow sampling in ATR mode. The background spectrum was collected prior analyzing each sample. Each IR spectrum reported herein is an average of four separate spectra, each consisting of 128 coadded scans at 4 cm^{-1} resolution. ATR-FTIR spectra were collected for (i) raw produced water after room temperature evaporation (ii) coagulated flocs from actual treated produced water (iii) precipitates formed in 28,000 mg/L NaCl solution containing 120 mg/L boron, i.e. positive control (iv) precipitates formed in 28,000 mg/L NaCl solution containing no boron, i.e. negative control.

2.4. XPS. The surface elemental composition of the flocs was measured using an Omnicron X-ray photoelectron spectrometer equipped with Argus detector and DAR 400 dual Mg/Al source. The moist paste obtained after centrifugation was washed several times using ultrapure water to reduce the amount of sorbed chloride ions since the B 1s peak is highly susceptible to interference from Cl 2p peak. After multiple washings, the paste was vacuum dried and then ground to fine powder before pressing it on a 0.25 mm thick indium substrate. High resolution B 1s, O 1s, Fe 2p and Al 2p spectra in the 0-1400 eV range were obtained to analyze their respective functionalities after calibrating electron binding energies with respect to adventitious carbon at 285 eV.

2.5. TEM. Flocs were sonicated to accommodate the small volume required for TEM. Although this leads to floc breakage, it is reasonably assumed that images of the fragmented flocs will be representative of the actual flocs because of their fractal nature [33, 34]. After sonication, 10 μL sample was pipetted and then placed on a 200 mesh

copper grid with carbon support films, dried at room temperature and imaged using a JEOL 1200 EX microscope.

2.6. X-ray diffractometry. Iron and aluminum polymorphs precipitated *in situ* were examined on a Bruker D8 advance X-ray diffractometer. The air-dried paste was deposited uniformly on a sample holder and diffraction patterns were collected using Cu kα radiation (1.54056 Å) at 40 kV and 40 mA. Diffractograms were collected in the 4° to 70° 2θ range with a step size of 0.019° 2θ/s, which were interpreted using the Joint Committee for Powder Diffraction Studies database.

2.7. Particle size distributions. An electrical sensing zone device (Multisizer 3, Beckman coulter, Miami, FL) was used to measure size distributions of flocs using a 1,000 μm aperture tube. Coagulated samples were diluted 100 fold using prefiltered 2% NaCl solution to reduce coincidence errors. Suspensions were gently stirred during the analysis to reduce sedimentation and floc breakage. The instrument was calibrated using NIST-certified 90 μm polystyrene beads and operated at a current of 3200 μA and gain of 1. Each analysis was completed in 30 seconds by drawing 150 mL of sample through the aperture tube.

2.8. Quality control and quality assurance. Several experiments were repeated and mass balances were performed on boron after coagulation. These results, which are summarized in Appendix C denote accurate and precise measurements and reproducible conduct of experiments allowing comparison of data generated over the entire duration of this study.

3. RESULTS AND DISCUSSION

3.1. Spectroscopic characterization of the flowback water. Due to the high strength and complex chemical composition of the flowback water, parameters reported in Table 1 were also qualitatively verified by FTIR and XPS. Prior to XPS, 500 ml of the produced water was nanofiltered (NF270, Dow Chemical) to selectively remove chloride since its high concentration overwhelmed other elements in X-ray spectra. A thick layer of material was deposited on the permselective membrane consistent with nanofiltration capturing a substantial fraction of the flowback water components. The morphology of the solids visualized under an electron microscope (top panel in Figure 1) suggested the dominance of inorganic precipitates as expected from the composition summarized in Table 1 and in our recently report [20].
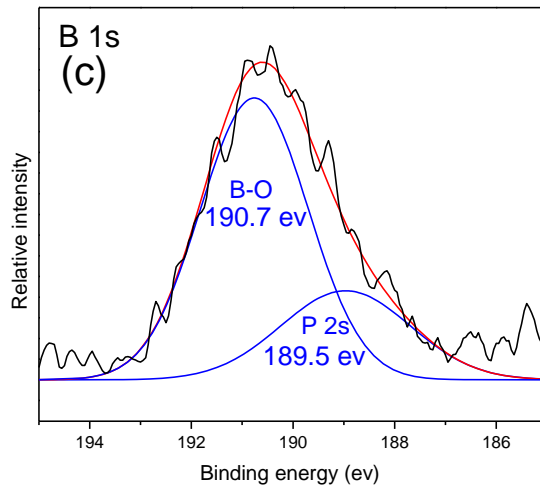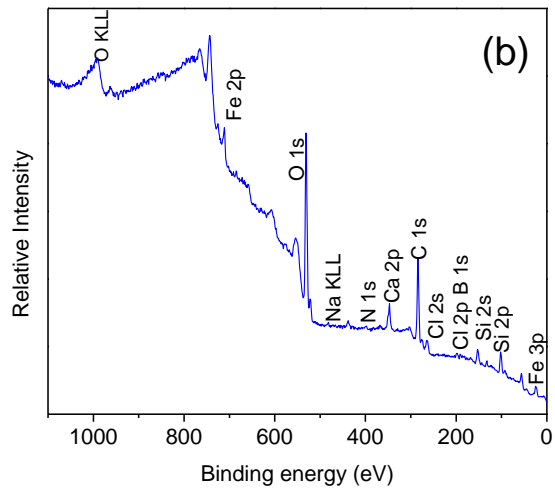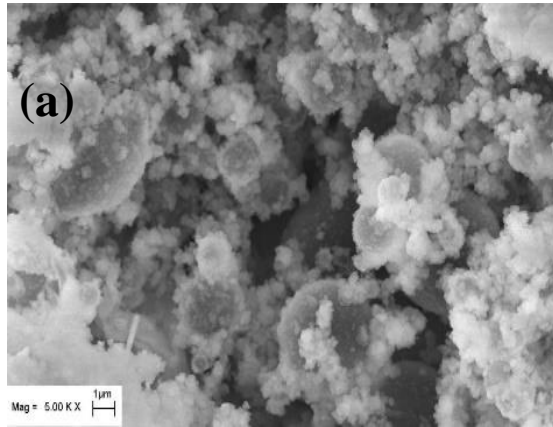
Figure 1. Hydraulic fracturing components captured by nanofiltration membrane: SEM image (a), XPS survey scan (b), high resolution scan for boron (c).

XPS wide scans identified C, O, and Si as the major elements with weaker signals for B, Ca, Fe, N, and S consistent with Table 1. Faint Cl signals are the consequence of preferred chloride ion passage through the nanofilter allowing the detection of other trace produced water components. The high resolution B 1s spectrum was deconvoluted into a B-O peak at 190.7 eV and another at 189.5 eV representing either P 2s (since P was detected in Table 1) or elemental boron [35].

The ATR-FTIR spectrum in the 1600 – 800 cm^{-1} range (see orange colored spectrum at the top of Figure 6 and Figure 7) also revealed several inorganic constituents including silica (νSi-O-Si 830cm^{-1}, νSi-O 1100cm^{-1}), boron compounds (νB-O-B 1340cm^{-1}, νB-O 1000cm^{-1}), carbonates (νCO$_3^{2-}$ 1456cm^{-1}), coordinated carbonates (νCO$_3^{2-}$ 1600-1540cm^{-1}, νC-O 960cm^{-1}) and sulfates (ν_{as}S-O 1064cm^{-1}) providing supplementary evidence for the composition reported in Table 1 and Figure 1b [36]. Stretching vibrations were also obtained from aliphatic and aromatic carbon representing organic compounds.

3.2. Boron removal by coagulation. As depicted in Figure 2, boron removal was maximized at a pH of 8 when neutral boric acid is dominant, and by increasing the dosage. Hence, similar to electrocoagulation, the highest uptake of boron onto iron and aluminum hydroxides during conventional chemical coagulation also occurred at a slightly alkaline pH. This is consistent with the pH where negatively charged aluminum (Al(OH)$_4^-$) becomes dominant and when iron solubility increases [25, 37, 38]. Also, for any given dosage and pH, aluminum slightly outperformed iron in terms of boron removal. Similar results were reported by other investigators for the same operating

11

conditions, where aluminum achieved slightly (~5%) higher removal than iron [25, 39]. This is attributed to the higher specific capacity of amorphous aluminum hydroxide compared with amorphous iron hydroxide to boron [40]. Since high dosages of aluminum and iron were necessary to substantially remove boron, large quantities of sludge was also formed necessitating residuals handling. For example, at 3,000 mg/L coagulant dosage, approximately 10 g/L sludge was generated in our experiments.
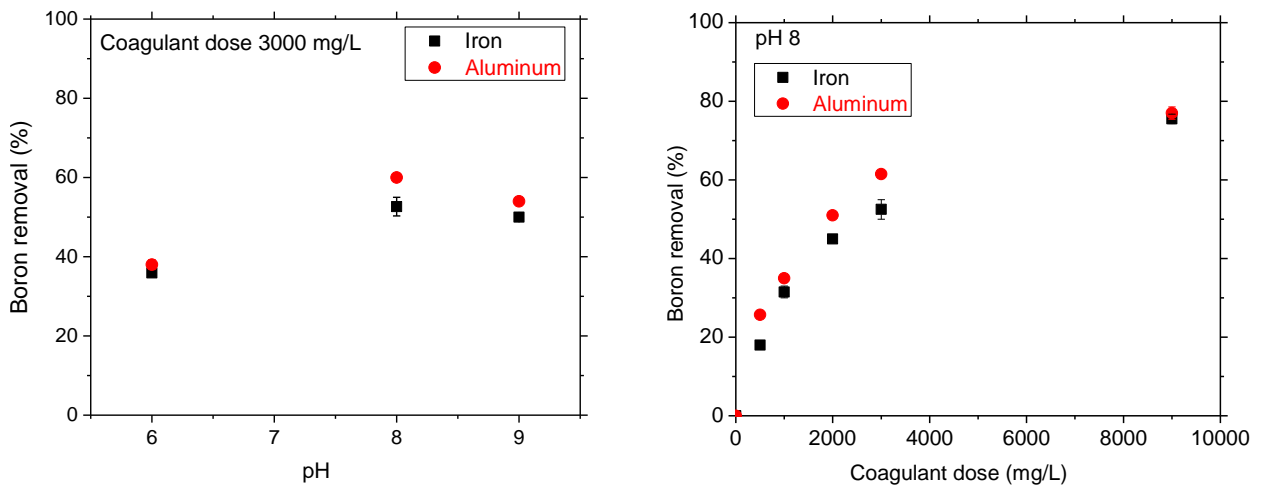
Figure 2. Effects of coagulation pH and coagulant dosage on boron removal.

3.3. Floc physical characteristics. The volume-weighted mean diameter (Figure 3a) and the cumulative volume of flocs increased with coagulant dosage demonstrating favorable precipitation conditions and formation of larger flocs as more and more iron and aluminum were added. TEM images showed the fractal nature of aluminum (Figure 3b) and iron (Figure 3c) flocs as shown by several other investigators e.g. [33, 34, 41]. Also in Figure 3, iron flocs can be seen to be denser than their aluminum counterparts as reported earlier [42, 43] resulting in their facile sedimentation. For example, at 3,000 mg/L dosage, iron flocs needed only 5 minutes for near-complete sedimentation whereas

aluminum flocs needed nearly 45 minutes.
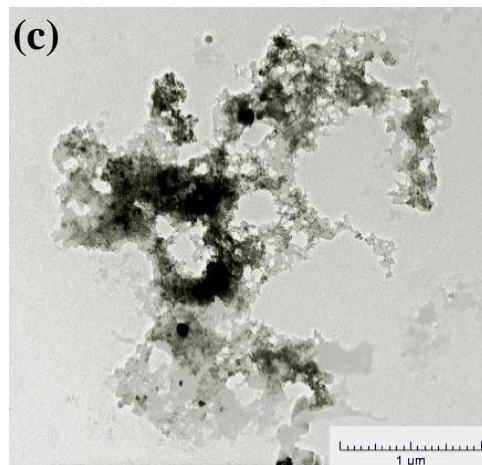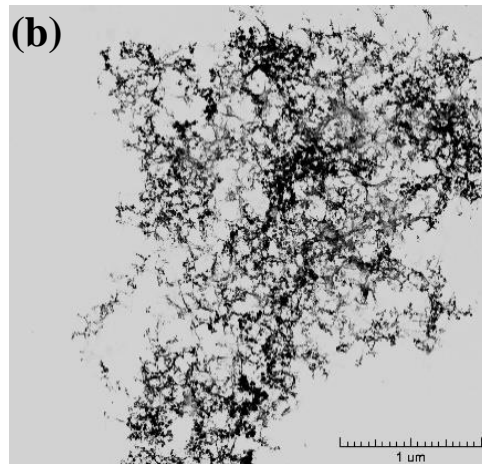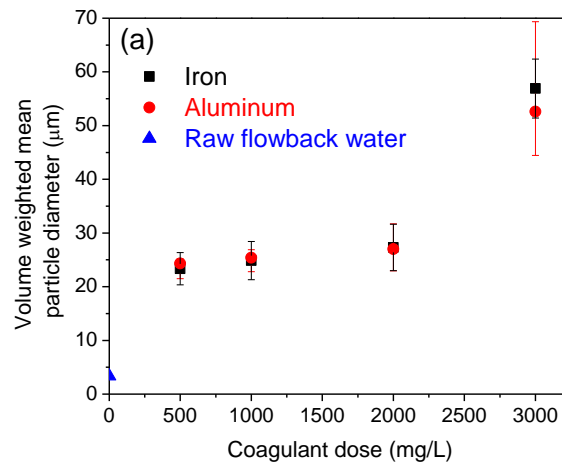
Figure 3. Size distributions of flocs (a) and TEM images at pH 8 and 3000 mg/L of aluminum (b) and iron flocs (c).

Narrow scan XPS was performed on solids harvested from coagulated flowback water. The Al 2p spectrum revealing a sharp peak at 74.6 eV demonstrating $Al(OH)_3$ precipitation during alum coagulation as seen in Figure 4a [44], which was confirmed by a hydroxyl peak at 532.1 eV in the O 1s spectrum [45]. In contrast, two peaks at 710 eV and 724 eV were obtained for iron coagulation corresponding to Fe $2p_{3/2}$ and Fe $2p_{1/2}$ respectively as depicted in Figure 4b [46]. Additionally, the Fe $2p_{3/2}$ was narrower and more intense than Fe $2p_{1/2}$ characteristic of Fe(III) oxidation state and Fe-O bonding [46, 47]. A hydroxyl peak was seen in the O 1s spectrum for iron flocs at 531.5 eV corresponding to $Fe(OH)_3$ precipitation [48].
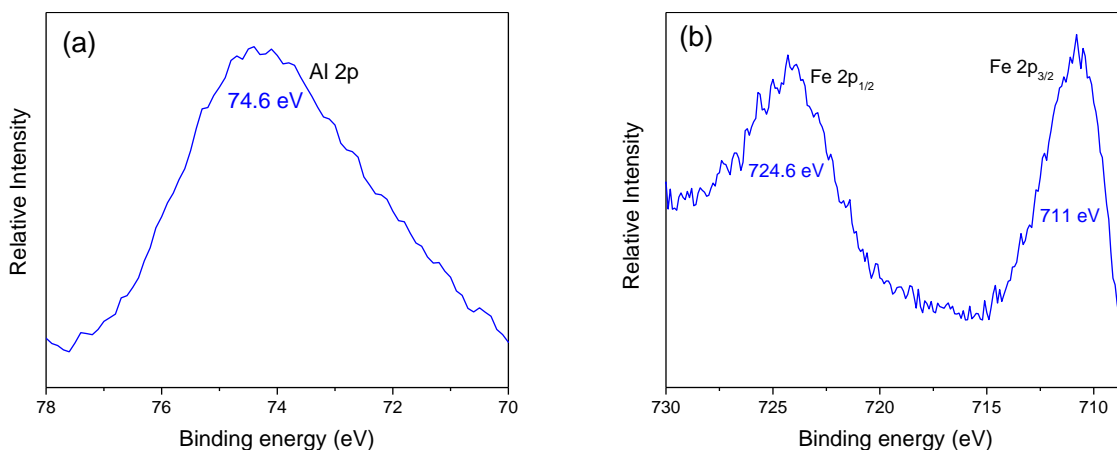
Figure 4. High resolution scans of Al 2p and Fe 2p from flocs generated by coagulation of the flowback water.

The nature of iron and aluminum hydroxide polymorphs generated *in situ* was further probed by XRD. A wide hump, characteristic of fluorescence signals arising from amorphous $Fe(OH)_3$ can be seen in Figure 5a, with only strong halite peaks arising from the high salt content of the flowback water. The diverging slit allowed passage of

photons at low angles leading to the sharp linear increase in intensity. In contrast, photons reflected at higher angles were blocked causing the intensity to decrease. Similarly, aluminum also showed only strong halite peaks (Figure 5b) confirming its amorphous nature. The amorphous nature of flocs produced in highly saline hydraulic fracturing wastewater is similar to those freshly precipitated in other water treatment applications [49-52]. This is consistent with sorption of boron, organic matter, and other components (section 3.6), which would have retarded crystallization of highly ordered phases [53-55].
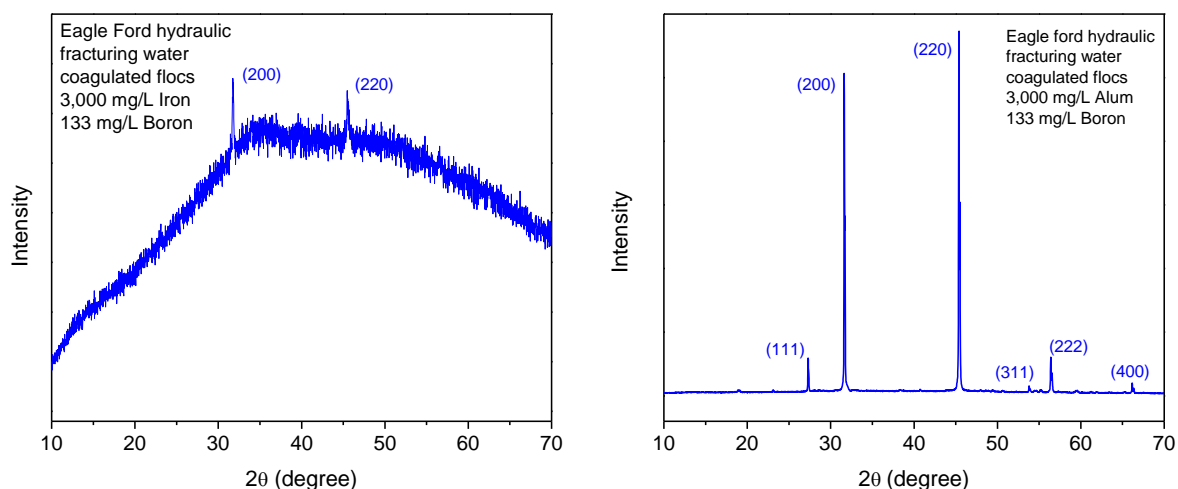
Figure 5. X-ray diffractograms of iron and aluminum hydroxide flocs formed in hydraulic fracturing wastewater.

Surfaces of iron and aluminum hydroxide flocs generated at pH 8 and dosage of 3000 mg/L were examined by high resolution XPS and ATR-FTIR to elucidate boron uptake mechanisms as described next.

3.4. Boron uptake on Al(OH)3 flocs. Narrow scan B 1s spectra for alum coagulated model solution (28,000 mg/L NaCl containing 120 mg/L B) and actual hydraulic

15

fracturing wastewater are shown in Figure 6a and Figure 6b respectively. A single B-O

peak at 191 eV effectively explained sorbed boron in both cases with no evidence for

direct Al-B bonding (i.e. no peak near 188 eV) [56]. Hence, boron uptake appears to be

via complexation with surface hydroxyl groups [19, 20, 57].
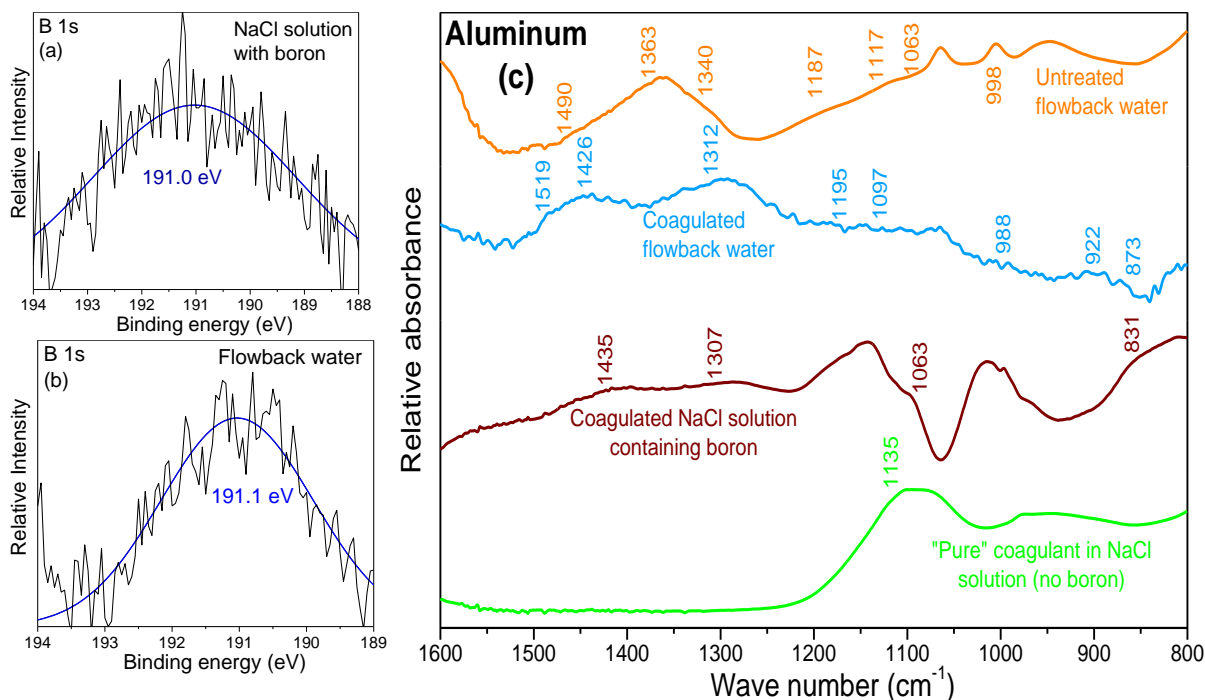
Figure 6. High resolution XPS scan for B 1s in alum coagulated produced water (left panel). ATR-FTIR spectra of Al(OH)$_3$ precipitates in NaCl solution without boron (green), Al(OH)$_3$ precipitates in a NaCl solution containing 100 mg/L boron (brown), flocs generated by coagulating the actual produced water (blue), and the raw produced water sample without coagulation (orange) are shown in the right panel.

ATR-FTIR analysis provided direct evidence of boron complexation with surface

hydroxyl groups (Figure 6). First, only a carbonate peak at 1135 cm^{-1} was observed in

Al(OH)$_3$ precipitated in NaCl solution with no boron (green color curve). This spectrum

was subtracted from IR spectra of other alum coagulated waters to remove background

signals. The brown and blue colored spectra correspond to alum coagulated NaCl

solution containing 120 mg/L boron and the actual flowback water. These spectra show two new peaks (1435 and 1307 cm^{-1} for NaCl solution and 1426 and 1312 cm^{-1} for flowback water) depicting trigonally coordinated boron with Al(OH)$_3$. While the peak close to 1430 cm^{-1} arises due to B-O asymmetric stretching, the peak near 1310 cm^{-1} is assigned to in-plane bending of trigonal boron [58]. Blueshifting compared to pure boric acid (1410 and 1148 cm^{-1}) indicates strengthening of O-B and B-OH bonds in the complex formed on coagulant surfaces [58]. Dominance of trigonal boron on Al(OH)$_3$ floc surfaces at pH 8 of our experiments is expected since the pK$_a$ of boric acid is 9.4 and suggests that neutral B(OH)$_3$ has higher affinity towards the neutral Al(OH)$_3$ surface as compared to the negatively charged B(OH)$_4^-$ species. The 1430 cm^{-1} peak suggests outer sphere complexation when boron behaves as a Lewis acid accepting an electron from oxygen on floc surfaces [58]. The peak around 1310 cm^{-1} suggests inner sphere complexation initiated by a ligand exchange mechanism leading to formation of a strong Al-O-B bond [58]. It was not feasible to probe tetrahedral boron ($\sim$ 925 cm^{-1}) during aluminum coagulation due to severe Al-O-Al and Al-O interferences in the wave number range 1100-680 cm^{-1}. Note that the raw flowback water spectrum (in orange) has already been discussed in section 3.1.

3.5. Boron uptake on Fe(OH)3 flocs. High resolution XPS of iron hydroxide flocs also revealed a B 1s peak at 191 eV demonstrating its uptake by from the model solution (Figure 7a) and the flowback water (Figure 7b). This corresponds to B-O bonding [56] and no evidence was obtained for direct Fe-B bonding (i.e. no peaks near 188 eV) [59].

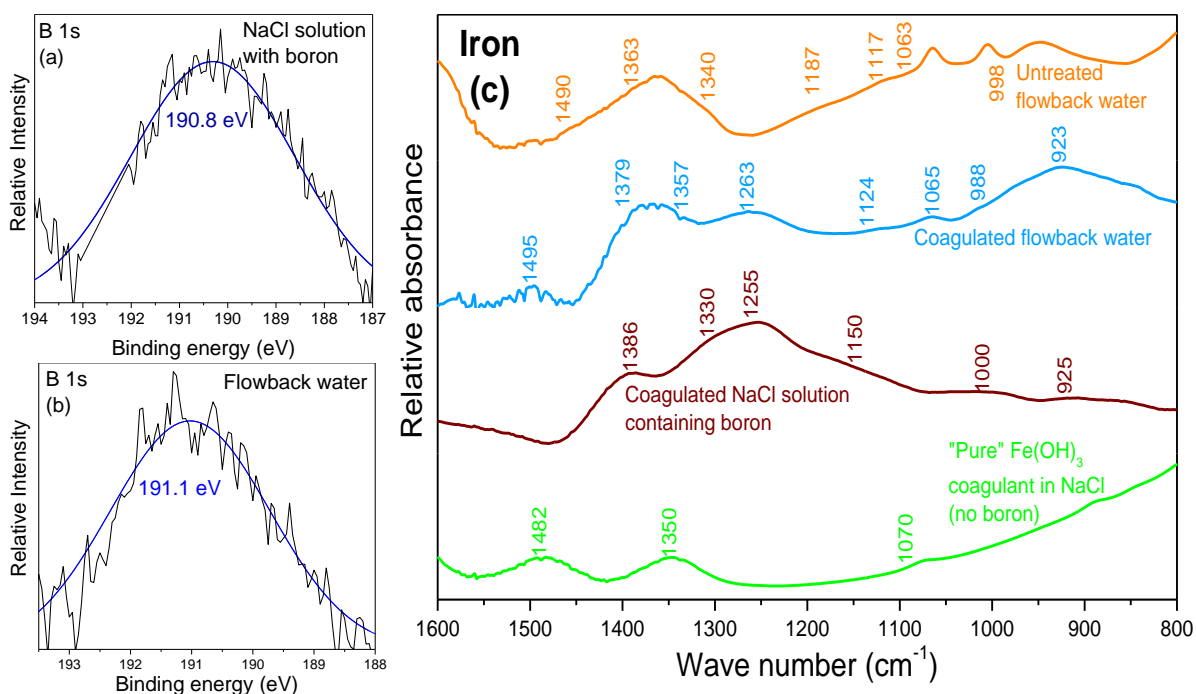Hence, similar to alum, ligand exchange appears to dominate boron uptake onto iron flocs [19, 20, 57].

Figure 7. High resolution XPS scan for B 1s in iron coagulated produced water (left panel). ATR-FTIR spectra of Fe(OH)$_3$ precipitates in NaCl solution without boron (green), Fe(OH)$_3$ precipitates in a NaCl solution containing 100 mg/L boron (brown), flocs generated by coagulating the actual produced water (blue), and the raw produced water sample without coagulation (orange) are shown in the right panel.

Boron sorption mechanisms were further investigated by ATR-FTIR spectroscopy as depicted in Figure 7c. The top spectrum (in orange) has already been discussed in section 3.1. Similar to alum, the IR spectrum for iron precipitates in 28 g/L NaCl solution containing no boron (in green) showed only carbonate peaks. This negative control spectrum was subtracted from IR spectra of other coagulated waters to remove background signals. Three subtle peaks were observed in difference spectra of iron flocs (in brown) generated in the model solution at 1386, 1330, 1255 cm^{-1} and the

actual flowback water (in blue) at 1379, 1357, 1263 cm^{-1} corresponding to trigonal coordination of boron with $Fe(OH)_3$ [60]. Outer-sphere complexation, arising from Lewis acidity of boron was evidenced in the form of B-O-H inplane bending near 1380 cm^{-1} [60]. Hydrogen bonding between hydroxyl groups on the iron surface and boric acid strengthens the outer sphere complex eventually even displacing water leading to formation of inner sphere complexes on coagulant surfaces [60]. Evidence for this behavior in the synthetic water was obtained as peaks near 1330 cm^{-1} and 1250 cm^{-1} arising from asymmetric stretching of B-O bonds formed via inner sphere complexation [60]. Blueshifting to 1357 cm^{-1} from 1330 cm^{-1} and to 1263 cm^{-1} from 1255 cm^{-1} for the flowback wastewater is attributed to carbonates and the strengthening of bonds on the surface complex. Also as reported earlier, a B-O symmetric stretching peak near 1000 cm^{-1} was not present at pH 8 [60]. Tetrahedral conformation of boron complexes on $Fe(OH)_3$ surfaces was also observed near 925 cm^{-1} since iron presented no interferences in this region [58]. Appendix D summarizes possible monomeric aluminum and iron surface complexes based on spectroscopic data.

3.6. Sorption of other flowback water components. Additional peaks in IR spectra (1200-900 cm^{-1}) of flocs harvested from hydraulic fracturing wastewater compared with that of "pure" coagulant precipitates in saline solution (Figure 6 and Figure 7) provide evidence for the uptake of organic carbon, silica, sulfate, and calcium along with boron. The relative atomic percentage of numerous other wastewater components (e.g. C, Si, Ca, and Mg) also increased compared to the pure coagulant in XPS survey scans confirming IR results (see Figure 8). DOC removal was independently measured to be

35% and 30% for iron and aluminum, respectively confirming organic carbon uptake by flocs. Turbidity in the clarified water was 3.1 NTU for iron and 2.1 NTU for aluminum corresponding to ~97% removal. Hence, conventional chemical coagulation is capable of removing a wide spectrum of contaminants from flowback water.
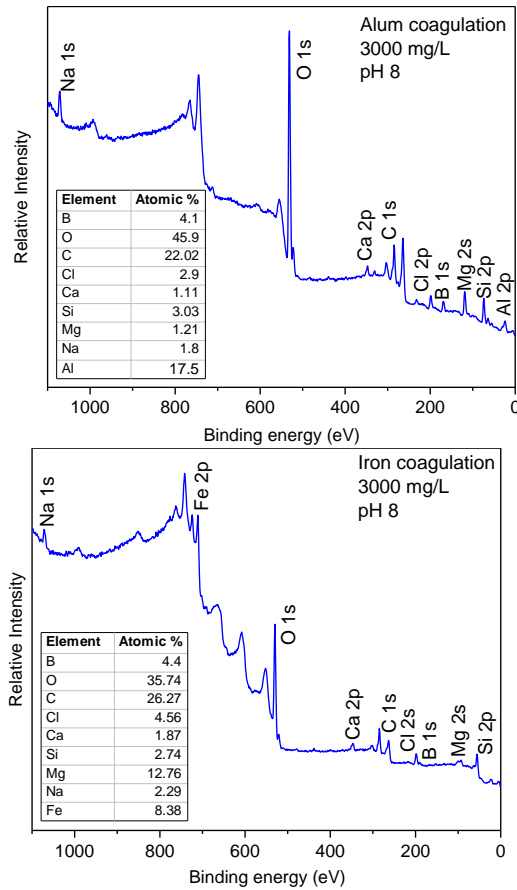
Figure 8. XPS survey scans of aluminum and iron flocs along with their relative atomic percentages showing the sorption of many flowback water components on their surfaces.

4. CONCLUSIONS

Hydrolyzing metal ion coagulants such as alum and iron chloride can effectively remove suspended solids and boron. Turbidity removal was close to 97% resulting in clarified water having values less than approximately 3 NTU. Alum slightly outperformed iron (by ~5%) for boron removal, which was maximized at a slightly alkaline pH of 8 and by increasing coagulant dosage. It is emphasized that very high coagulant dosages were necessary to achieve high boron removals (Al/B and Fe/B ratios > 75 for ~ 80% removal). Concomitantly, large amounts of sludge are produced requiring careful disposal considerations. In this study, for an aluminum or iron dosage of 3 g/L, approximately 10 g/L of sludge was formed.

XPS demonstrated a ligand exchange mechanism of boron uptake on hydroxide surfaces. ATR-FTIR spectroscopy provided direct evidence for inner and outer sphere complexation of boron on surfaces of amorphous aluminum and iron hydroxides. IR spectra detected both trigonally and tetrahedrally coordinated boron with iron hydroxide surfaces. In contrast, only trigonal boron was observed on aluminum hydroxide surfaces due to heavy interferences from Al-O bonds, which absorb in the same wave number range as tetrahedrally coordinated boron.

Wide XPS scans detected the presence of other produced water components including carbonaceous organic matter, hardness, and silica on floc surfaces. Hence, conventional coagulation also appears to non-specifically remove several constituents in oil-field waste streams.

Evaluation of other coagulants such as polyaluminum chloride (PACl) for oil-field wastewater treatment is recommended for the future. PACl might be advantageous since it hydrolyzes to form highly charged polymeric alumino-hydroxyl species that can directly neutralize colloidal charge. Additionally, the $Al(OH)_3$ precipitates formed by PACl addition are more densely packed and incorporate less water allowing faster sedimentation compared to alum flocs. Another recommendation is to perform detailed characterization of dissolved organic carbon in flowback water before and after coagulation to evaluate the treatability of individual components. Given the numerous, proprietary additives employed for fracking, in addition to physicochemical characterization of treated waters, its toxicity also needs to be evaluated prior to irrigation

REFERENCES

1.   Scanlon, B.R., R.C. Reedy, and J.P. Nicot, *Comparison of water use for hydraulic fracturing for unconventional oil and gas versus conventional oil.* Environmental Science & Technology, 2014. **48**(20): p. 12386-12393.

2.   Vidic, R.D., S.L. Brantley, J.M. Vandenbossche, D. Yoxtheimer, and J.D. Abad, *Impact of shale gas development on regional water quality.* Science, 2013. **340**(6134): p. 1235009:1-9.

3.   Elsner, M. and K. Hoelzer, *Quantitative survey and structural classification of hydraulic fracturing chemicals reported in unconventional gas production.* Environmental Science & Technology, 2016. **50**(7): p. 3290-3314.

4.   Gregory, K.B., R.D. Vidic, and D.A. Dzombak, *Water management challenges associated with the production of shale gas by hydraulic fracturing.* Elements, 2011. **7**(3): p. 181-186.

5.   Piñero, E., *Total water cycle management for hydraulic fracturing in shale gas production*, in *Hydraulic Fracturing: Environmental Issues. ACS Symposium Series Volume 1216*, D.L. Drogos, Editor. 2015, American Chemical Society: Washington D.C. p. 129-133.

6.   Vengosh, A., R.B. Jackson, N. Warner, T.H. Darrah, and A. Kondash, *A critical review of the risks to water resources from unconventional shale gas development and hydraulic fracturing in the United States.* Environmental Science & Technology, 2014. **48**(15): p. 8334-8348.

7.   Camarillo, M.K., J.K. Domen, and W.T. Stringfellow, *Physical-chemical evaluation of hydraulic fracturing chemicals in the context of produced water treatment.* Journal of Environmental Management, 2016. **183**: p. 164-174.

8.   Shariq, L., *Uncertainties Associated with the Reuse of Treated Hydraulic Fracturing Wastewater for Crop Irrigation.* Environmental Science & Technology, 2013. **47**(6): p. 2435-2436.

9.   Greenhill-Hooper, M.J., *Oilfield technology and applications involving borates*, in *Boron Science: New Technologies and Applications*. 2011. p. 417-447.

10.   Reid, R.J., J.E. Hayes, A. Post, J.R. Stangoulis, and R.D. Graham, *A critical analysis of the causes of boron toxicity in plants.* Plant, Cell & Environment, 2004. **27**(11): p. 1405-1414.

11.   U.S.E.P.A, *Drinking water: Health advisory for boron and compounds*, D.H. Health and Ecological Criteria, Office of Science and Technology (OST), Office of Water (OW), Office of Groundwater/Drinking Water (OGWDW), OW, U.S. EPA, Editor. 2008.

12.   WHO, *Boron in drinking water*. 2003, WHO/SDE/WSH/03.04.54 (http://www.who.int/water_sanitation_health/dwq/boron.pdf): Geneva, Switzerland.

13.   Murray, F.J., *A human health risk assessment of boron (boric acid and borax) in drinking water.* Regulatory Toxicology and Pharmacology, 1995. **22**(3): p. 221-230.

14. Wang, B., X. Guo, and P. Bai, *Removal technology of boron dissolved in aqueous solutions – A review.* Colloids and Surfaces A: Physicochemical and Engineering Aspects, 2014. **444**: p. 338-344.

15. Xu, P., J.E. Drewes, and D. Heil, *Beneficial use of co-produced water through membrane treatment: Technical-economic assessment.* Desalination, 2008. **225**(1-3): p. 139-155.

16. Xu, Y. and J.-q. Jiang, *Technologies for boron removal.* Industrial & Engineering Chemistry Research, 2008. **47**: p. 16-24.

17. Wolska, J. and M. Bryjak, *Methods for boron removal from aqueous solutions — A review.* Desalination, 2013. **310**: p. 18-24.

18. Karahan, S., M. Yurdakoc, Y. Seki, and K. Yurdakoc, *Removal of boron from aqueous solution by clays and modified clays.* Journal of Colloid and Interface Science, 2006. **293**(1): p. 36-42.

19. Theiss, F.L., G.A. Ayoko, and R.L. Frost, *Removal of boron species by layered double hydroxides: A review.* Journal of Colloid and Interface Science, 2013. **402**: p. 114-121.

20. Sari, M.A. and S. Chellam, *Mechanisms of boron removal from hydraulic fracturing wastewater by aluminum electrocoagulation.* Journal of Colloid and Interface Science, 2015. **458**: p. 103-111.

21. Davis, C.C. and M. Edwards, *Coagulation With Hydrolyzing Metal Salts: Mechanisms and Water Quality Impacts.* Critical Reviews in Environmental Science and Technology, 2014. **44**(4): p. 303-347.

22.   Pourrezaei, P., P. Drzewicz, Y.N. Wang, M.G. El-Din, L.A. Perez-Estrada, J.W. Martin, J. Anderson, S. Wiseman, K. Liber, and J.P. Giesy, *The impact of metallic coagulants on the removal of organic compounds from oil sands process-affected water.* Environmental Science & Technology, 2011. **45**(19): p. 8452-8459.

23.   Ezechi, E.H., M.H. Isa, S.R.M. Kutty, and A. Yaqub, *Boron removal from produced water using electrocoagulation.* Process Safety and Environmental Protection, 2014. **92**(6): p. 509-514.

24.   Jiang, J.-Q., Y. Xu, K. Quill, J. Simon, and K. Shettle, *Mechanisms of boron removal with electrocoagulation.* Environmental Chemistry, 2006. **3**(5): p. 350-354.

25.   Sayiner, G., F. Kandemirli, and A. Dimoglo, *Evaluation of boron removal by electrocoagulation using iron and aluminum electrodes.* Desalination, 2008. **230**(1-3): p. 205-212.

26.   Yilmaz, A.E., R. Boncukcuoğlu, M.M. Kocakerim, M.T. Yilmaz, and C. Paluluoğlu, *Boron removal from geothermal waters by electrocoagulation.* Journal of Hazardous Materials, 2008. **153**(1-2): p. 146-151.

27.   Isa, M.H., E.H. Ezechi, Z. Ahmed, S.F. Magram, and S.R.M. Kutty, *Boron removal by electrocoagulation and recovery.* Water Research, 2013. **51**: p. 113-123.

28.   Vasudevan, S. and J. Lakshmi, *Electrochemical removal of boron from water: Adsorption and thermodynamic studies.* The Canadian Journal of Chemical Engineering, 2012. **90**(4): p. 1017-1026.

29.   Denne, R.A., R.E. Hinote, J.A. Breyer, T.H. Kosanke, J.A. Lees, N. Engelhardt-Moore, J.M. Spaw, and N. Tur, *The Cenomanian-Turonian Eagle Ford group of South Texas: Insights on timing and paleoceanographic conditions from geochemistry and micropaleontologic analyses.* Palaeogeography Palaeoclimatology Palaeoecology, 2014. **413**: p. 2-28.

30.   Wang, L., J.D. Fortner, and D.E. Giammar, *Impact of water chemistry on element mobilization from Eagle Ford shale.* Environmental Engineering Science, 2015. **32**(4): p. 310-320.

31.   Cengeloglu, Y., G. Arslan, A. Tor, I. Kocak, and N. Dursun, *Removal of boron from water by using reverse osmosis.* Separation and Purification Technology, 2008. **64**(2): p. 141-146.

32.   ASTM, *Annual book of ASTM standards section 11*, in *Standard Test Methods for Boron in Water* 1985, ASTM International: Philadelphia. p. 353-359.

33.   Lee, S.Y. and G.A. Gagnon, *Growth and structure of flocs following electrocoagulation.* Separation and Purification Technology, 2016. **163**: p. 162-168.

34.   Harif, T., M. Khai, and A. Adin, *Electrocoagulation versus chemical coagulation: Coagulation/flocculation mechanisms and resulting floc characteristics.* Water Research, 2012. **46**(10): p. 3177-3188.

35.   Eyhusen, S., C. Ronning, and H. Hofsass, *Phase formation of boron nitride thin films under the influence of impurity atoms.* Diamond and Related Materials, 2003. **12**(3-7): p. 1173-1177.

36.   Dahm, K.G., K.L. Guerra, P. Xu, and J.E. Drewes, *Composite geochemical database for coalbed methane produced water quality in the rocky mountain region.* Environmental Science & Technology, 2011. **45**(18): p. 7655-7663.

37.   Yilmaz, A.E., R. Boncukcuoğlu, and M.M. Kocakerim, *A quantitative comparison between electrocoagulation and chemical coagulation for boron removal from boron-containing solution.* Journal of Hazardous Materials, 2007. **149**(2): p. 475-481.

38.   Lindsay, W.L. and A.P. Schwab, *The chemistry of iron in soils and its availability to plants.* Journal of Plant Nutrition, 1982. **5**(4-7): p. 821-840.

39.   Goldberg, S. and R.A. Glaubig, *Boron adsorption on aluminum and iron-oxide minerals.* Soil Science Society of America Journal, 1985. **49**(6): p. 1374-1379.

40.   Tagliabue, M., A.P. Reverberi, and R. Bagatin, *Boron removal from water: Needs, challenges and perspectives.* Journal of Cleaner Production, 2014. **77**: p. 56-64.

41.   Chakraborti, R.K., K.H. Gardner, J.F. Atkinson, and J.E. Van Benschoten, *Changes in fractal dimension during aggregation.* Water Research, 2003. **37**(4): p. 873-883.

42. Larue, O. and E. Vorobiev, *Floc size estimation in iron induced electrocoagulation and coagulation using sedimentation data.* International Journal of Mineral Processing, 2003. **71**(1-4): p. 1-15.

43. Tambo, N. and Y. Watanabe, *Physical characteristics of flocs. 1. Floc density-function and aluminum floc.* Water Research, 1979. **13**(5): p. 409-419.

44. Strohmeier, B.R., *An ESCA method for determining the oxide thickness on aluminum-alloys.* Surface and Interface Analysis, 1990. **15**(1): p. 51-56.

45. Kloprogge, J.T., L.V. Duong, B.J. Wood, and R.L. Frost, *XPS study of the major minerals in bauxite: Gibbsite, bayerite and (pseudo-)boehmite.* Journal of Colloid and Interface Science, 2006. **296**(2): p. 572-576.

46. Grosvenor, A.P., B.A. Kobe, M.C. Biesinger, and N.S. McIntyre, *Investigation of multiplet splitting of Fe 2p XPS spectra and bonding in iron compounds.* Surface and Interface Analysis, 2004. **36**(12): p. 1564-1574.

47. Yamashita, T. and P. Hayes, *Analysis of XPS spectra of Fe^{2+} and Fe^{3+} ions in oxide materials.* Applied Surface Science, 2008. **254**(8): p. 2441-2449.

48. Biesinger, M.C., B.P. Payne, A.P. Grosvenor, L.W.M. Lau, A.R. Gerson, and R.S. Smart, *Resolving surface chemical states in XPS analysis of first row transition metals, oxides and hydroxides: Cr, Mn, Fe, Co and Ni.* Applied Surface Science, 2011. **257**(7): p. 2717-2730.

49. Berkowitz, J., M.A. Anderson, and R.C. Graham, *Laboratory investigation of aluminum solubility and solid-phase properties following alum treatment of lake waters.* Water Research, 2005. **39**(16): p. 3918-3928.

50.   Gamage, N.P. and S. Chellam, *Aluminum electrocoagulation pretreatment reduces fouling during surface water microfiltration.* Journal of Membrane Science, 2011. **379**(1-2): p. 97-105.

51.   Gunnars, A., S. Blomqvist, P. Johansson, and C. Andersson, *Formation of Fe(III) oxyhydroxide colloids in freshwater and brackish seawater, with incorporation of phosphate and calcium.* Geochimica et Cosmochimica Acta, 2002. **66**(5): p. 745-758.

52.   Chafi, M., B. Gourich, A.H. Essadki, C. Vial, and A. Fabregat, *Comparison of electrocoagulation using iron and aluminium electrodes with chemical coagulation for the removal of a highly soluble acid dye.* Desalination, 2011. **281**: p. 285-292.

53.   Masion, A., J.Y. Bottero, F. Thomas, and D. Tchoubar, *Chemistry and structure of Al(OH)/Organic precipitates-A small angle X-ray-scattering study. 2. Speciation and structure of the aggregates* Langmuir, 1994. **10**(11): p. 4349-4352.

54.   Cornell, R.M. and U. Schwertmann, *Influence of organic-anions on the crystallization of ferrihydrite.* Clays and Clay Minerals, 1979. **27**(6): p. 402-410.

55.   Beyrouty, C.A., G.E. Vanscoyoc, and J.R. Feldkamp, *Evidence supporting specific adsorption of boron on synthetic aluminum hydroxides.* Soil Science Society of America Journal, 1984. **48**(2): p. 284-287.

56. Xu, D. and D. Peak, *Adsorption of boric acid on pure and humic acid coated am-Al (OH)₃: A boron K-edge XANES study.* Environmental Science & Technology, 2007. **41**(3): p. 903-908.

57. Ren, Z.M., G.S. Zhang, and J.P. Chen, *Adsorptive removal of arsenic from water by an iron-zirconium binary oxide adsorbent.* Journal of Colloid and Interface Science, 2011. **358**(1): p. 230-237.

58. Su, C. and D.L. Suarez, *Coordination of adsorbed boron: A FTIR spectroscopic study.* Environmental Science & Technology, 1995. **29**(2): p. 302-311.

59. Huntley, D.R., S.H. Overbury, D.M. Zehner, J.D. Budai, and W.E. Brower Jr, *Surface characterization of amorphous and crystallized Fe₈₀B₂₀.* Applied Surface Science, 1986. **27**(2): p. 180-198.

60. Peak, D., G.W. Luther, and D.L. Sparks, *ATR-FTIR spectroscopic studies of boric acid adsorption on hydrous ferric oxide.* Geochimica et Cosmochimica Acta, 2003. **67**(14): p. 2551-2560.
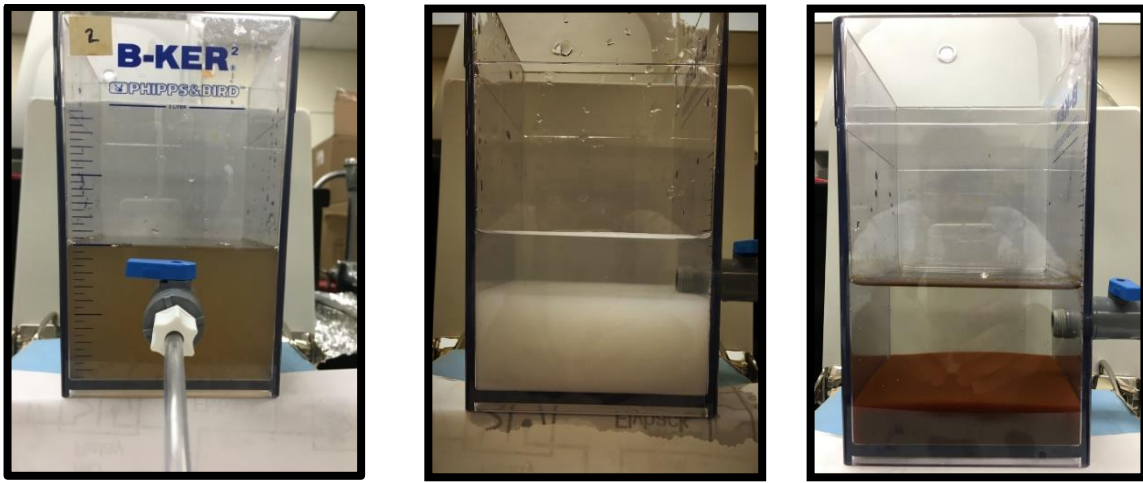
APPENDIX A

Figure 9. The programmable Phipps and Bird jar tester used for all experiments.

Figure 10. Photographs of the raw flowback water (left), after coagulation-flocculation-sedimentation using alum (middle) and iron chloride (right). A sludge layer separated from the clear supernatant is visible for both alum and iron visually demonstrating successful clarification.

APPENDIX C

Quality control and quality assurance statements. First, 5 different boron concentrations (10, 30, 50, 70, and 100 mg/L) were spiked in 28,000 mg/L NaCl solution and measured by D-mannitol titration to within 1.2% accuracy. Second, a 28,000 mg/L NaCl solution was spiked with 120 mg/L boron and coagulated at 5 different conditions of pH and iron and aluminum dosages. For each of these experiments, boron was measured in the feed water and supernatant by titration. Then, the flocs were dissolved by adding HCl to depress the pH and boron was measured in the acidified sample using ICP-OES to determine the sorbed amount. Boron recovery in these 5 experiments was $99.6 \pm 1.9\%$. Third, using the same floc-dissolution procedure, boron was quantitatively recovered ($98.5 \pm 2.5\%$) from the actual hydraulic fracturing water sample. Finally, the relative percentage difference in boron removal from five duplicate experiments conducted under different pH values and iron and aluminum dosages was only $5.9 \pm 2.6\%$. The relative percentage difference was calculated as the difference between the theoretical and measured values normalized by the theoretical value expressed as a percentage. These QA/QC tests demonstrate accurate and precise boron measurements and reproducible conduct of experiments allowing comparison of data generated over the entire duration of this study.

APPENDIX D

Boron sorption mechanisms

Table 2. Schematic representation of boron coordination complexes on iron hydroxides (from [58]). Note that we only found evidence for trigonal complexes on aluminum due to severe interferences.

Trigonally coordinated boron complexes with aluminum	$B(OH)_3^0 (aq) + \equiv AlOH^0 (s) \rightleftharpoons \equiv Al{-}O{-}B(OH){-}OH(s) + H_2O (l)$ $B(OH)_3^0 (aq) + \equiv AlOH_2^+ (s) \rightleftharpoons \equiv Al{-}O{-}B(OH){-}OH(s) + H_2O (l) + H^+ (aq)$ $B(OH)_4^- (aq) + \equiv AlOH (s) \rightleftharpoons \equiv Al{-}O{-}B(OH){-}OH(s) + H_2O (l) + OH^- (aq)$
Trigonally coordinated boron complexes with iron	$B(OH)_3^0 (aq) + \equiv FeOH^0 (s) \rightleftharpoons \equiv Fe{-}O{-}B(OH){-}OH (s) + H_2O (l)$ $B(OH)_3^0 (aq) + \equiv FeOH_2^+ (s) \rightleftharpoons \equiv Fe{-}O{-}B(OH){-}OH (s) + H_2O (l) + H^+ (aq)$ $B(OH)_4^- (aq) + \equiv FeOH (s) \rightleftharpoons \equiv Fe{-}O{-}B(OH){-}OH (s) + H_2O (l) + OH^- (aq)$
Tetrahedrally coordinated boron complexes with iron	$B(OH)_3^0 (aq) + 2\equiv FeOH (s) \rightleftharpoons \equiv (Fe{-}O)_2{-}B(OH)_2 (s) + H_2O (l) + H^+ (aq)$ $B(OH)_4^- (aq) + 2\equiv FeOH^0 (s) \rightleftharpoons \equiv (Fe{-}O)_2{-}B(OH)_2 (s) + 2H_2O (l)$